DOI:
10.4155/fmc-2019-0329

Document Version
Peer reviewed version

Radiolabelling of [^{11}C]FPS-ZM1, a RAGE-targeting PET radiotracer, using a [^{11}C]CO_2-to-[^{11}C]CO chemical conversion.

Federico Luzi,[1] Vilius Savickas,[1,2*] Carlotta Taddei,[1*] Stefan Hader,[1] Nisha Singh,[1,3] Antony D. Gee[1@*] and Salvatore Bongarzone[@1*]*

1. School of Biomedical Engineering and Imaging Sciences, King's College London, 4th Floor, Lambeth Wing, St. Thomas' Hospital, Westminster Bridge Road, London, SE1 7EH, UK.

2. National Institute for Health Research Biomedical Research Centre at Guy's and St Thomas' NHS Foundation Trust and King's College London, 16th Floor, Tower Wing, Guy's Hospital, Great Maze Pond, London, SE1 9RT, UK.

3. Centre for Neuroimaging Sciences, Institute of Psychiatry, Psychology and Neuroscience, King's College London, 16 De Crespigny Park, London, SE5 8AF, UK.

** These authors equally participated to this work.*

@ antony.gee@kcl.ac.uk, salvatore.bongarzone@kcl.ac.uk

KEYWORDS

RAGE

Carbon-11

PET imaging

FPS-ZM1

Alzheimer's Disease

[^{11}C]CO radiochemistry

Silanecarboxylate derivatives

ABSTRACT

Background: The receptor for advanced glycation endproducts (RAGE) is a viable target for early AD diagnosis using positron emission tomography (PET) as RAGE overexpression preceeds Aβ plaque formation. The development of a carbon-11 analogue of FPS-ZM1 ([^{11}C]FPS-ZM1), possessing nanomolar affinity for RAGE, may enable the imaging of RAGE for early AD detection. **Methodology/Results:** Herein we report an optimized [^{11}C]CO_2-to-[^{11}C]CO chemical conversion for the synthesis of [^{11}C]FPS-ZM1 and *in vitro* brain autoradiography. The [^{11}C]CO_2-to-[^{11}C]CO conversion *via* ^{11}C-silanecarboxylate derivatives was achieved with a 57% yield within 30 seconds from EOD. [^{11}C]FPS-ZM1, was obtained with a decay-corrected isolated RCY of 9.5%. **Conclusions:** [^{11}C]FPS-ZM1 distribution in brain tissues of wild-type versus transgenic AD-model mice showed no statistically-significant difference and high non-displaceable binding.

INTRODUCTION

Alzheimer's disease (AD) is the most common subtype of dementia, however is misdiagnosed in 30-60% of all cases.[1, 2] Positron emission tomography (PET) enables real-time imaging of brain function[3] and AD clinical diagnosis.[4] The use of PET may enable the early detection of AD, possibly even 25 years before the onset of the first symptoms.[5]

The current diagnosis of AD with PET focuses on imaging insoluble beta amyloid (Aβ) plaques using radiotracers such as fluorine-18 (^{18}F)-labelled flutemetamol ([^{18}F]flutemetamol, 2-[3-[^{18}F]fluoro-4-(methyl-amino)-phenyl]-6-benzothiazolol)[6] and carbon-11 (^{11}C)-labelled Pittsburgh compound B ([^{11}C]PiB, 2-(4'-[^{11}C]methylaminophenyl)-6-hydroxybenzothiazole).[7] The deposition of insoluble Aβ plaques, however, almost certainly occurs too late in the AD disease process for successful therapeutic intervention and also does not always correlate with AD diagnosis or loss of cognition[8, 9] thus limiting the diagnostic

utility of Aβ-targeting radiotracers.[10, 11] An alternative strategy aims at detecting hyperphosphorylated tau protein, the main component of the neurofibrillary tangles (NFTs),[12] *via* the use of specific radiotracers such as [^{18}F]T808.[13] Nevertheless, the accumulation of tau NFTs is also observed in frontotemporal dementia,[14] and, additionally, may not be present in sufficient amounts to be accurately detected by PET until late stage disease.[15] Therefore, to provide an accurate early diagnosis of AD as well as progress in drug development, new radiotracers targeting early pathophysiological pathways are crucial.[16, 17] The overexpression of the receptor for advanced glycated endproducts (RAGE) is linked with AD progression[16, 18] and could represent an alternative strategy for AD imaging. The extracellular region of RAGE binds several endogenous ligands, such as S100 calcium-binding proteins, advanced glycation endproducts (AGEs) and Aβ peptides and oligomers.[16] The binding of neurotoxic Aβ oligomers to RAGE mediates the pre-pathological neurodegenerative inflammatory process[19] and triggers AD-related effects, including enhanced activity of Aβ-producing β-secretase enzyme 1 (BACE1),[20, 21] tau hyperphosphorylation,[22] and increased influx of Aβ across the blood brain barrier (BBB).[18, 21] Moreover, RAGE activation induces an overexpression of the receptor itself as shown in the brain of patients with advanced AD compared to mild AD or healthy controls.[17, 23] In a transgenic mouse model of AD (Tg2576) expression of RAGE was highest at the age of 15 months.[21, 24, 25]

The pathological role of RAGE inspired the development of numerous inhibitors able to block the binding of Aβ to its V domain,[16] limiting the detrimental downstream effects. Among these inhibitors, a potent small molecule able to selectively bind the V domain of RAGE is the tertiary amide-based FPS-ZM1 (*N*-benzyl-4-chloro-*N*-cyclohexylbenzamide, **Figure 1**). FPS-ZM1 possesses nanomolar affinity for RAGE (inhibitory constant K_i = 25 ± 5 nM)[21] and a good *in vivo* safety profile.[21] *In vitro*, FPS-ZM1 is able to reduce RAGE-mediated cellular oxidative stress, BACE1 mRNA and activity, and nuclear NF-κB levels.[21] In 15-to-18

month-old Tg2576 mice, FPS-ZM1 (intraperitoneally administered, 1 mg/kg daily for 2 months) showed a high brain uptake, a decreased influx of Aβ at the BBB to the brain with restored cognitive function and cerebral blood flow.[21]

Based on the good *in vitro* and *in vivo* selectivity towards RAGE,[21] FPS-ZM1 was selected as a starting structure for the development of RAGE-targeting PET radiotracers. An ^{18}F radiolabelled tracer ([^{18}F]fluoro-FPS-ZM1, **Figure 1**) has been developed by substituting the chlorine atom of FPS-ZM1 with fluorine-18 (clogP = 4.9).[26][27] Regional time-activity curves in non-human primates and wild type (WT) rodents showed a rapid brain uptake and a slow elimination from hippocampal regions[26] – consistent with known RAGE expression.[17] Although these *in vivo* results showed a good uptake in healthy animals, an assessment in a Tg2576 mouse model might more accurately predict the biodistribution profile of the RAGE radiotracer in a pathological state. Moreover, the use of ^{11}C allows the authentic labelling of the unmodified compound, retaining its pharmacodynamic and pharmacokinetic profile. A ^{11}C-labelled analogue of FPS-ZM1 ([^{11}C]FPS-ZM1) was therefore developed for testing with AD animal models.

Here we report the incorporation of carbon-11 into the tertiary amide moiety of FPS-ZM1 *via* a ^{11}C-amidation reaction using [^{11}C]carbon monoxide ([^{11}C]CO) as synthon. [^{11}C]CO is a versatile synthon that is easily incorporated into a vast array of ^{11}C-carbonyl-containing molecules, such as ^{11}C-amides.[27-29] Cyclotron-produced ^{11}C is usually obtained in the form of [^{11}C]carbon dioxide ([^{11}C]CO_2) and converted to [^{11}C]CO by: *i)* gas-phase reduction,[30] *ii)* electrochemical conversion,[31] or *iii)* chemical conversion *via* ^{11}C-silanecarboxylate derivatives. The latter methodology was recently translated to ^{11}C-chemistry to produce [^{11}C]CO *via* a one-step chemical reaction between [^{11}C]methyldiphenylsilanecarboxylate ([^{11}C]**1**) and tetrabutylammonium fluoride (TBAF) (**Figure 2**) by heating (60 °C) resulting in in a modest [^{11}C]CO_2-to-[^{11}C]CO conversion (38 ± 8%).[32]

The aims of this work were to: *i)* optimise the [^{11}C]CO_2-to-[^{11}C]CO conversion *via* [^{11}C]**1** by studying the variables involved in the [^{11}C]CO production such as temperature, reaction time, reagent stability and sample preparation; *ii)* employ the produced [^{11}C]CO to radiolabel [*carbonyl*-^{11}C]FPS-ZM1 ([^{11}C]FPS-ZM1, **Figure 1**); and *iii)* assess [^{11}C]FPS-ZM1 *in vitro* in the brains of wild type (WT) *versus* Tg2576 mice.

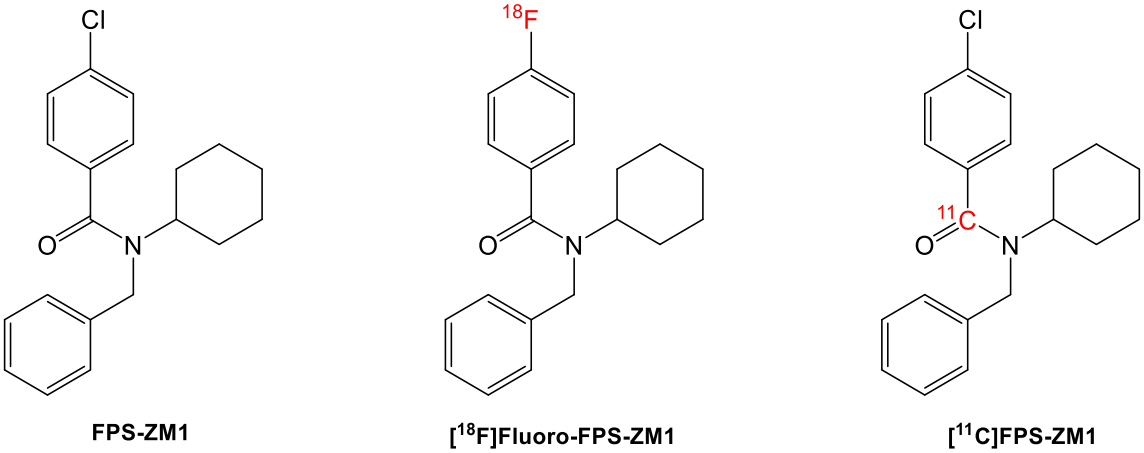

Figure 1. Chemical structures of the RAGE inhibitor FPS-ZM1, [^{18}F]fluoro-FPS-ZM1 and [^{11}C]FPS-ZM1.

EXPERIMENTAL SESSION

General Method and Materials

All chemicals and dry solvents were purchased from Sigma-Aldrich and Alfa Aesar and used as received. Crimp caps (centre hole with 3.0 mm PTFE, seal in aluminium silver 20 mm, Fisherbrand, 10132712) and oven-dried reaction v-vial (KX Microwave Vials) were used. All the lines used to allow the passage of gases were PTFE tubing (length: 10–20 cm, O.D.: 0.79 x 0.4 in., I.D.: 1/32 x 0.16 in.). RCYs are based on initial radioactivity of [^{11}C]CO_2 and decay corrected from EOD.

General Procedure for the Preparation of 3

2 was added into an oven-dried argon-flushed vial (Vial P) containing lithium and dry THF (1.8 mL). The reaction vial was sealed and stirred for 3-24 h at 20 °C under argon. Vial P was centrifuged (Jouan, CR 412) at 15 °C and 7000 rpm for 10 min. Subsequently, two aliquots (0.45 mL) were transferred under an argon atmosphere (glovebox) to oven-dried argon-flushed V-vials (Vial A).

Animals

All procedures involving animals were conducted in accordance with European Commission's Directive 2010/63/EU. The animals were used in accordance with ethical principles of Replacement, Reduction and Refinement.[33] All experiments were performed in tissues of 17-month-old Tg2576 (n=2) and 8-month-old WT CD-1 (n = 4) mice.

Preparation of Tissues

Animals underwent anaesthesia with isoflurane (2%) and were sacrificed by decapitation 5 minutes later. Organs were harvested in isopentane, wrapped in foil and frozen to -80 °C. Sagittal 20 µm brain sections were prepared using MNT cryostat (SLEE Medical, Germany) as previously described.[7, 26] Two to four sections were mounted onto each SuperFrost® Plus blue 90° ground microscopy slide (catalog no. 631-0446, VWR International, UK) and stored at -80 °C.

Autoradiography

After the synthesis, [^{11}C]FPS-ZM1 was reformulated using a Sep-Pack Light C18 cartridge and redissolved in a 9:1 water:ethanol mixture. Slides for TB and NDB were defrosted to room temperature (2 h prior the incubation), rehydrated in tris-buffered saline (10 min; TBS, pH 7.6) and then incubated at room temperature in separate Coplin jars (20 min; catalog no. 12858735,

Fisher Scientific, UK) containing TBS, the same concentration of [^{11}C]FPS-ZM1 (1-20 nM) and either dimethyl-sulfoxide for TB or FPS-ZM1 (10-75 μM) for NDB. Following incubation, they were washed in TBS (2 min) and rinsed in deionised water. Slides were then fan-dried and exposed to a phosphor imaging plate (30 min; BAS-IP TR 2040, GE Healthcare, UK). The plate was scanned using a Typhoon 8600 phosphorimager (GE Healthcare, UK).

Images were analysed using OptiQuant 5.0 software (PerkinElmer, UK). Cerebellum and whole brain region of interests (ROIs) were drawn manually. Qualitative analysis was conducted to determine any visual differences between ROIs and animal strains. Quantitative binding was expressed as mean normalised digital line units (DLU)/mm^2 ± standard deviation. Data was analysed using Microsoft Excel 2016 and GraphPad Prism (7.0d). SB was estimated as a difference between TB and NDB. All SB data was expressed as % of WT whole brain region. WT cerebellum was normalized to whole brain WT to compare the uptake of the tracer in the cerebellum relatively to the whole brain. Independent t-tests (statistical significance $p<0.05$) were carried out to compare the variables across ROIs and animal strains.

RESULTS AND DISCUSSION

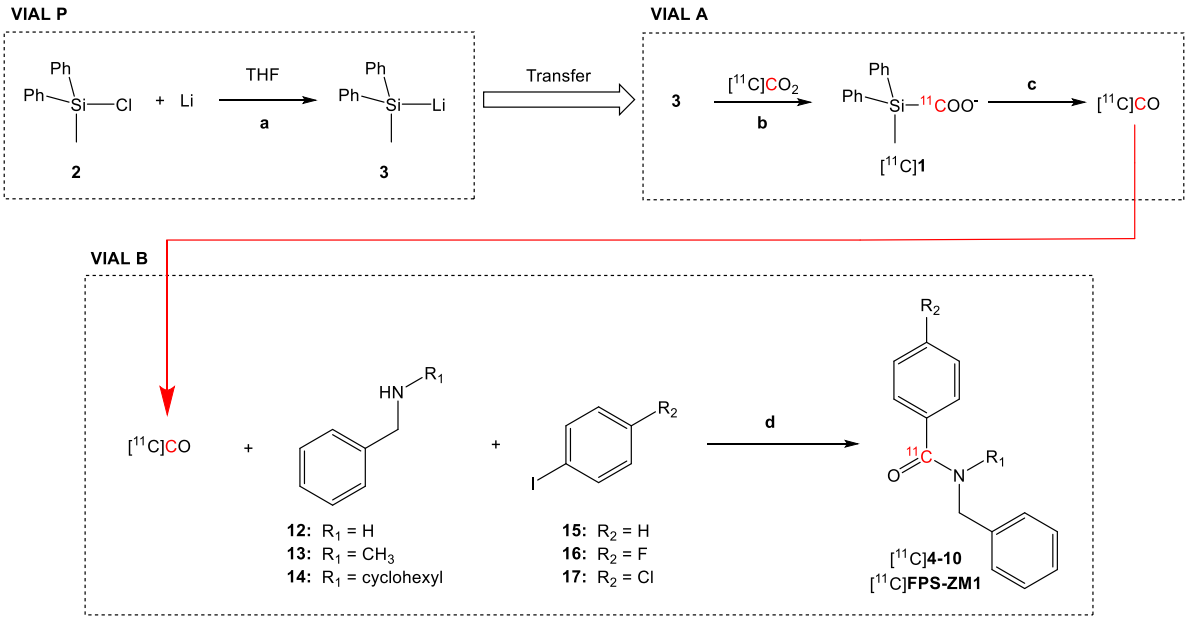

Figure 2. a. Vial P: Li (1.73 mmol), **2** (0.64 mmol), THF (1.8 mL), 3h, r.t. After 3h, an aliquot of Vial P (0.22 – 0.9 mL) is transferred in Vial A, which is used for the $[^{11}C]CO_2$ trapping. **b.** Vial A: $[^{11}C]CO_2$, r.t., 2 min. **c.** TBAF (0.8 mmol) added in Vial A, then transfer of $[^{11}C]CO$ from Vial A to Vial B with a helium gas stream (60 mL/min). **d.** Vial B: **12**-**14** (0.24 mmol), **15**-**17** (0.01 mmol), $[(cinnamyl)PdCl]_2$ (0.007 mmol), xantphos (0.007 mmol), solvent (450 µL), 40-120 °C, 2-5 min.

Optimization of the $[^{11}C]CO_2$-to-$[^{11}C]CO$ conversion *via* $[^{11}C]$**1**

In our previous report, the $[^{11}C]CO_2$-to-$[^{11}C]CO$ conversion was performed in a single vial set-up (Vial A) yielding 38% of $[^{11}C]CO$ based on total cyclotron produced $[^{11}C]CO_2$ (entry 1, **Table 1**).[32] Briefly, **2** (0.32 mmol, 1.0 equiv., 0.35 mM) reacted with lithium (2.7 equiv.) in dry THF (900 µL) at room temperature for 3 h at 20 °C under inert gas atmosphere to give **3**. $[^{11}C]CO_2$ was subsequently bubbled into Vial A triggering the formation of $[^{11}C]$**1** (step **b**, **Figure 2**), which released $[^{11}C]CO$ by heating (60 °C) upon TBAF addition (step **c**, **Figure 2**). We hypothesized that the excess of unreacted lithium (black particles) contained in Vial A and the heating of Vial A were hampering the quantitative conversion of $[^{11}C]CO_2$ to $[^{11}C]CO$. To reduce the content of unreacted lithium, we opted for the synthesis of **3** in a preparation vial (Vial P). Vial P contained **2** (0.64 mmol, 1 equiv., 0.35 mM) and lithium (4 equiv.) in anhydrous THF (1.8 mL) and was stirred at room temperature for 3 hours to yield **3** (step **a**, **Figure 2**). Upon reaction completion, 0.45 mL of the supernatant of Vial P were transferred to an empty

oven-dried vial (Vial A) under inert gas atmosphere to be used for the [^{11}C]CO_2-to-[^{11}C]CO conversion to Vial A.

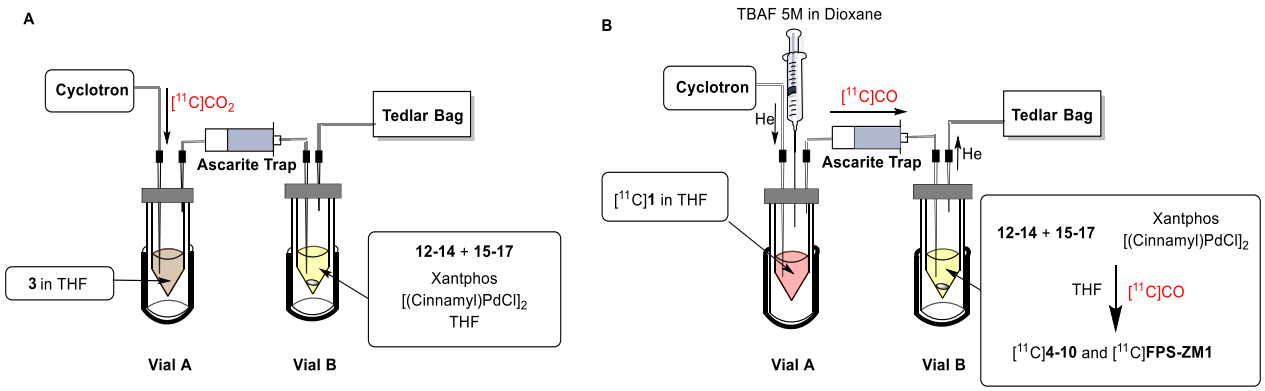

Figure 3. Set up of the two-vial system. **A.** [^{11}C]CO_2 is trapped by Vial A; **B.** TBAF addition in Vial A promotes the conversion of [^{11}C]**1** to [^{11}C]CO, which is transferred to Vial B with an helium flush. The transferred [^{11}C]CO will be consumed in Vial B for producing [^{11}C]**4**-**10** and [^{11}C]**FPS-ZM1**.

The cyclotron-produced [^{11}C]CO_2 was subsequently bubbled into Vial A with high trapping efficiency (> 99%, n = 100), leading to the formation of [^{11}C]**1** (step **b**, **Figure 2**). TBAF was added to Vial A at room temperature giving a 47% release of [^{11}C]CO from [^{11}C]**1** (entry 2, **Table 1**) within 10 seconds. Thus, excluding the unreacted lithium particles from the mixture and performing the TBAF addition at room temperature had a positive effect on [^{11}C]CO release, with an increase of [^{11}C]CO production of ~10% (38% in entry 1 *versus* 47% in entry 2, **Table 1**). With the aim of further increasing the production of [^{11}C]CO, we turned our attention to the preparation time of **3** by varying the reaction time between **2** and lithium. By decreasing the reaction time from 3 hours to 2, 1 and 0.5 hours, no variation on [^{11}C]CO release was observed (~50%, entries 3–5, **Table 1**). However, when the reaction between **2** and lithium was stirred for 0.2 h or 24 h (entries 6-7, **Table 1**), a detrimental decrease on [^{11}C]CO release (3% and 4%, respectively) was observed. A reaction time of 0.2 h might not be enough to obtain **3** in good yield, whilst a 24 h reaction formed high amounts of insoluble precipitate which might have a negative impact on [^{11}C]CO release. To eliminate the insoluble precipitate,

centrifugation of Vial P was performed before transferring part of the supernatant solution into Vial A. The centrifugation step increased the release of [^{11}C]CO from 4% (entry 7, **Table 1**) to 38% (entry 8, **Table 1**). Similarly, the centrifugation step increased the [^{11}C]CO release when **2** and lithium were stirred for 3 h (no centrifugation step: 47 ± 4 %, entry 2 *versus* centrifugation included: 57 ± 4%, entry 9, **Table 1**). Complete trapping of the cyclotron-produced [^{11}C]CO_2 was obtained in each case (> 98%). The centrifugation of Vial P before transferring part of the volume into Vial A had a positive effect on [^{11}C]CO production, thus being routinely implemented in the method, thereafter.

As a next step, we examined the effect of the amount of **2** (0.32-1.24 mmol) after either 3 hours (entries 10-11, **Table 1**) or 24 hours (entries 12-13, **Table 1**) of synthesis time. When the amount of **2** was lowered from 0.64 mmol to 0.32 mmol while keeping constant lithium equivalents, [^{11}C]CO production dropped from 57% to 8% after 3 hours (entries 9 and 10, **Table 1**) and from 38% to 14% after 24 hours (entries 8 and 12, **Table 1**). When the amount of **2** was increased from 0.64 mmol to 1.24 mmol, [^{11}C]CO production slightly decreased from 57% to 31% after 3 hours (entries 9 and 11, **Table 1**) but was unaffected when the reaction was stirred for 24 hours (entries 8 and 13, **Table 1**).

Further investigations focused on varying the volume of solution transferred form Vial P into Vial A whilst keeping constant the concentration of the reagents (0.36 mM of **2**). When a volume of 0.9 mL (entry 14, **Table 1**) or 0.225 mL (entry 15) rather than 0.45 mL (entry 9) was transferred, the production of [^{11}C]CO decreased from 57% to 38% and 42%, respectively.

Table 1. The effect of reagents amount, reaction time and preparation of Vail A on [^{11}C]CO release *via* [^{11}C]**1**.

Entry [a]	Amount of 2 (mmol)	Volume transferred (mL)	Hours	Centrifugation	% [^{11}C]CO released [b]
1[34]	0.64	-	3	No	38 ± 8%
2	0.64	0.45	3	No	47 ± 4 (5)
3	0.64	0.45	1	No	56
4	0.64	0.45	2	No	51

5	0.64	0.45	0.5	No	54
6	0.64	0.45	0.2	No	3
7	0.64	0.45	24	No	4
8	0.64	0.45	24	Yes	38 ± 3 (3)
9	0.64	0.45	3	Yes	57 ± 4 (15)
10	0.32	0.45	3	Yes	8
11	1.28	0.45	3	Yes	31
12	0.32	0.45	24	Yes	14
13	1.28	0.45	24	Yes	35
14	0.64	0.90	3	Yes	38
15	0.64	0.22	3	Yes	42

[a] **Vial P: 2 (1 equiv., 0.64 -1.28 mmol), lithium (4 equiv.), THF (1.8 mL). After 0.1-24 h, 0.22-0.9 mL of solution is transferred to Vial A. [^{11}C]CO_2 was delivered at 20 °C for 105 seconds into Vial A. Addition of TBAF 1 M in THF (0.8 mmol) after 30 sec of EOD. Vial B: [^{11}C]CO, 12 (0.46 mmol), 15 (0.01 mmol), [(cinnamyl)PdCl]$_2$ (0.007 mmol), xantphos (0.007 mmol), THF (0.5 mL), 25 °C.**

[b] The % [^{11}C]CO released was calculated dividing the amount of radioactivity in Vial B over the total radioactivity (Vial A + Vial B + ascarite trap) measured at the end of [^{11}C]CO production.

To further optimise the reaction, we focused on the effect on [^{11}C]CO release of varying the amount of TBAF added to [^{11}C]**1** and the interval times between TBAF addition and [^{11}C]CO_2 delivery. A range of TBAF concentrations (0.4-1.6 mmol, entries 1-3, **Table SI1**) were added to [^{11}C]**1** after 30 seconds from end of [^{11}C]CO_2 delivery (EOD). The use of 0.8 mmol of TBAF granted a [^{11}C]CO release of 57% (entry 1, **Table SI1**). Reducing or increasing the TBAF content to 0.4 or 1.6 mmol lowered the [^{11}C]CO release (24% and 19%, respectively, entries 2-3, **Table SI1**). Subsequently, a study on the interval (30 seconds, 5 and 30 minutes) between EOD and TBAF addition was performed. High [^{11}C]CO release was achieved when TBAF solution was added within 5 min from EOD (55%, entry 4, **Table SI1**). On the contrary, the addition of TBAF after 30 min from EOD gave low [^{11}C]CO yields (28%, entry 5, **Table SI1**) probably due to potential degradation of [^{11}C]**1** in the reaction mixture.

In summary, the highest [^{11}C]CO release from [^{11}C]**1** (57% (n = 15), entry 9, **Table 1**) was achieved when: *1)* 0.64 mmol (1 equiv.) of **2** reacted with lithium (4 equiv.) in 1.8 mL of THF for 3 hours at room temperature; *2)* 0.45 mL of the supernatant solution were transferred in

Vial A after centrifuging the reaction mixture contained in Vial P; *3)* the [^{11}C]CO_2 delivery into Vial A was performed at room temperature; and *4)* 0.8 mmol of TBAF were added 30 seconds post EOD.

Radiosynthesis of [^{11}C]4-10 and [^{11}C]FPS-ZM1

The optimized conditions for [^{11}C]CO production (entry 9, **Table 1**) were applied to the radiolabeling of [^{11}C]**4-10** and [^{11}C]**FPS-ZM1**. A second oven-dried v-shaped reaction vial (Vial B) was preloaded with Pd(π-cinnamyl)chloride ([(cinnamyl)PdCl]$_2$), xantphos, benzylamine (**12-14**) and iodobenzene (**15-17**) derivatives in anhydrous THF under nitrogen. (step **d**, **Figure 2**). Once [^{11}C]CO was transferred into Vial B, it was consumed in a Pd-mediated ^{11}C-carbonylation reaction forming ^{11}C-benzylbenzamide derivatives ([^{11}C]**4-10** and [^{11}C]**FPS-ZM1**).[32] A sodium hydroxide-coated silica (ascarite) trap was placed between the two vials to capture any untrapped [^{11}C]CO_2 (**Figure 2**).

The strategy to synthesize [^{11}C]FPS-ZM1 was developed starting from previous studies on an analogue compound ([^{11}C]benzylbenzamide, [^{11}C]**4**) obtained in high radiochemical yield (RCY > 99%) by coupling benzylamine (**12**) with iodobenzene (**15**).[32, 34] Compared to [^{11}C]**4** (**Table 2**), [^{11}C]FPS-ZM1 bears a tertiary amide, a bulky cyclohexyl group and a chlorine atom in *para*-position to the amide group. The influence of these chemical features was explored by combining primary and secondary amines (**12-14**, **Figure 3**, **Table 2**) with different *para*-iodo aryl halides (**15-17**).

Table 2. Effects of substituents R_1 and R_2 on RCY and chemical structures of the ^{11}C-labelled products

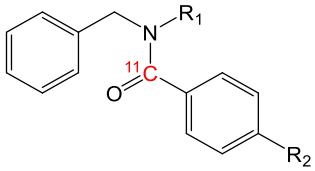

General structure of [^{11}C]**4-11**

Product	Amine	Iodobenzene	R_1	R_2	RCY (%) [a]
[^{11}C]**4**	**12**	**15**	H	H	>99% [b]
[^{11}C]**5**	**13**	**15**	CH_3	H	80% [b]
[^{11}C]**6**	**14**	**15**	cyclohexyl	H	37% [b]
[^{11}C]**7**	**12**	**16**	H	F	>99% [b]
[^{11}C]**8**	**14**	**16**	cyclohexyl	F	36% [b]
[^{11}C]**9**	**12**	**17**	H	Cl	74% [b]
[^{11}C]**10**	**13**	**17**	CH_3	Cl	52% [b]
[^{11}C]FPS-ZM1	**14**	**17**	cyclohexyl	Cl	30.2 ± 5.3% [c]

[a] 9-11 (0.24 mmol), 12-14 (0.01 mmol), [(cinnamyl)PdCl]$_2$ (0.007 mmol), xantphos (0.007 mmol), THF (450 µL), 5 min, 100 °C. RCY is the percentage of of product radioactivity divided by total radioactivity observed in an analytical HPLC chromatogram.
[b] n = 1;
[c] n = 12.

.

The substitution of a hydrogen atom of the benzylamine (**12**) with a methyl group (*N*-benzylmethylamine, **13**) aimed to elucidate the reactivity of a secondary amine substituted with a low sterically-hindered group. This modification lowered the RCY to 80% ([^{11}C]**5**, **Table 2**). The lowered reactivity is more pronounced when a bulkier cyclohexyl group (*N*-benzylcyclohexanamine, **14**) is introduced ([^{11}C]**6**, RCY = 37%).

The same trend was observed using *p*-iodo fluorobenzene (**16**) and *p*-iodo chlorobenzene (**17**). Indeed, when **16** reacted with **14**, the RCY was lower compared to the reaction with the least sterically-hindered **12** ([^{11}C]**8**, RCY = 36% *versus* [^{11}C]**7**, RCY > 99%, **Table 2**). **17** showed the same RCY decrease when coupled with **12** ([^{11}C]**9**, RCY = 74%), **13** ([^{11}C]**10**, RCY = 52%) and **14** ([^{11}C]**11**, RCY = 30.2%, **Table 2**). Thus, switching from a primary to a secondary amine and increasing the steric hindrance on the amine partly impedes the reaction irrespective of the *p*-iodoaryl halide derived used.

Varying the para substituent (R_2) of iodobenzene also affected the RCY of the reaction (**Table 2**). The presence of a hydrogen (**15**) or a fluorine (**16**) showed the same RCY when either

amines **12** ([^{11}C]**7**, RCY > 99% *versus* [^{11}C]**4**, RCY > 99%) or **14** ([^{11}C]**8**, RCY = 36% *versus* [^{11}C]**6**, RCY = 37%) were used.

The insertion of a chlorine atom (**17**) in *para* position of the iodobenzene instead significantly diminished the RCY of the reaction compared to **15** ([^{11}C]**9**, RCY = 74% *versus* [^{11}C]**4**, RCY > 99%; [^{11}C]**10**, RCY = 52% *versus* [^{11}C]**5**, RCY = 80%; [^{11}C]**FPS-ZM1**, RCY = 30% of *versus* [^{11}C]**6**, RCY = 37%, **Table 2**).

To increase the RCY of [^{11}C]**FPS-ZM1** (RCY = 30.2 ± 5.3%), different variables were also investigated: temperature, addition of a base, concentration of **14** and solvent (**Table SI2**).

Decreasing the temperature from 100 °C to 40 °C (entry 1, **Table SI2**) did not yield the product whereas increasing the temperature to 120 °C lowered the RCY from 30% to 14% (entry 2, **Table SI2**). The addition of a base, such as NEt_3, to increase the nucleophilicity of **14** was detrimental for the reaction (entry 3, **Table SI2**). Doubling the concentration of **14** from 0.24 mmol to 0.48 mmol did not improve the RCY (RCY = 14%, entry 4, **Table SI2**). Furthermore, solvents other than THF were tested: dioxane (RCY = 15%, entry 5, **Table SI2**) and acetonitrile (ACN, RCY = 9%, entry 6, **Table SI2**) were associated with a lower RCY of [^{11}C]**FPS-ZM1**.

In conclusion, the optimal conditions for [^{11}C]**FPS-ZM1** production are obtained when 0.24 mmol of **14** are reacted with 0.01 mmol of **17** at 100 °C in anhydrous THF for 5 minutes (**Table 2**). With these conditions, [^{11}C]**FPS-ZM1** was produced with a decay-corrected isolated RCY of 9.5 ± 1.5% and radiochemical purity (RCP) > 99% within 24 minutes from end of cyclotron target bombardment (EOD), resulting in an activity yield of 3.3 ± 1.4% based on an initial [^{11}C]CO production of ~100 MBq. The molar activity of the final product was 0.77 ± 0.13 GBq/µmol decay-corrected at EOD starting with an initial [^{11}C]CO_2 delivery of 300 MBq. This method was adopted for the synthesis of [^{11}C]FPS-ZM1 to be tested in *in vitro* experiments.

Autoradiography

One of the key requirements for a central nervous system PET radiotracer is high binding affinity towards its molecular target and low non-specific binding.[35, 36] The binding profile of [^{11}C]**FPS-ZM1** against RAGE was evaluated in brain sections of WT and 17-month Tg2576 mice.

The binding was assessed in the whole brain (minus cerebellum) and the cerebellum. Total binding (TB) was confirmed at varying concentrations of [^{11}C]**FPS-ZM1** (5-10 nM) whereas non displaceable binding (NDB) was determined in the presence of differing concentration of non-radioactive FPS-ZM1 (25-75 μM). Specific binding (SB) was obtained by subtracting the signal of NDB from TB.

Qualitative and quantitative analysis was conducted at three sets of concentrations (**A**-**C**):

A: TB: 10 nM of [^{11}C]**FPS-ZM1** and NDB: 10 nM of [^{11}C]FPS-ZM1 with 25 μM of FPS-ZM1; **B**: TB: 10 nM of [^{11}C]**FPS-ZM1** and NDB: 10 nM of [^{11}C]**FPS-ZM1** with 75 μM of FPS-ZM1; **C:** TB: 5 nM of [^{11}C]**FPS-ZM1** and NDB: 5 nM of [^{11}C]**FPS-ZM1** with 75 μM of FPS-ZM1.

Qualitative image analysis using 10 nM of [^{11}C]**FPS-ZM1** showed high NDB of [^{11}C]**FPS-ZM1** (sets **A** and **B**) in WT and Tg2576 mice. By lowering the concentration of [^{11}C]**FPS-ZM1** from 10 nM to 5 nM (set **C**), a lower degree of NDB was observed in WT and Tg2576 mice (**Figure 3A**). Thus, set **C** was chosen for quantitative autoradiography analysis to enable a comparison with qualitative images.

Although qualitative images showed an increase in SB of [^{11}C]**FPS-ZM1** in the whole brain of Tg2576 *versus* WT mice (49%, **Figure 3A-B**), this difference was not statistically significant when a quantitative autoradiography analysis was performed (**Figure 3B**).

Figure 4. A. Qualitative autoradiography comparison of TB and NDB signals in WT and Tg2576 at concentration set C. **B**. SB of [^{11}C]**FPS-ZM1** in WT and Tg2576 mouse brain normalised to WT whole brain at concentration set C. Set C: TB: 5 nM of [^{11}C]**FPS-ZM1** and NDB: 5 nM of [^{11}C]**FPS-ZM1** with 75 μM of FPS-ZM1.

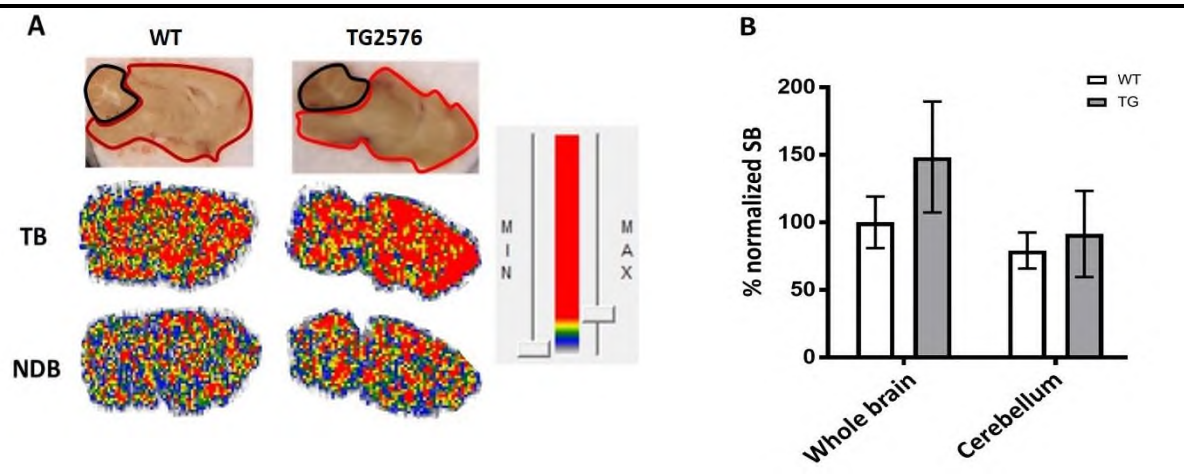

All values are expressed as % WT whole brain SB ± standard deviation and were derived from 3 independent quantitative autoradiography experiments. WT cerebellum value was normalized to the whole brain SB. The black-circled area indicates the cerebellum, whereas the red-circled area is the whole brain (minus cerebellum). Autoradiographic images are displayed according to the NIH intensity scale for tracer activity, from red (highest), through green (intermediate) to blue (lowest).

CONCLUSION

In summary, a rapid and reliable method for the chemical conversion of [^{11}C]CO_2 to [^{11}C]CO *via* [^{11}C]**1** at room temperature was achieved with a [^{11}C]CO release of up to 57% within 30 seconds from EOD based on total radioactivity delivered. The produced [^{11}C]CO was employed for the synthesis of a novel ^{11}C-PET-based RAGE radiotracer *via* Pd-catalyzed [^{11}C]CO amidation, [^{11}C]**FPS-ZM1**, which was obtained with a decay-corrected isolated RCY of 9.5%. The *in vitro* evaluation of [^{11}C]**FPS-ZM1** showed a 49% greater SB signal in the whole brain of Tg2576 *versus* WT mice, however this was non-statistically significant. Moreover, a high degree of NDB was observed. Poor radiotracer displacement may be explained by its high lipophilicity (calculated LogP for FPS-ZM1 = 5.25)[37] leading to increased NDB to lipids (*e.g.* cell membrane).[38] This barrier may be overcome by modifying the lipophilicity of future radiotracers derived from this pharmacophore for imaging RAGE.

FUTURE PERSPECTIVES

Although at present AD progression cannot be halted or reversed, the availability of a RAGE radiotracer for PET imaging would enable the monitoring of brain RAGE levels from presymptomatic to late stage AD and establish a temporal relationship between neuroinflammation, RAGE expression, amyloid-β plaque and neurofibrillary tangle formation as well as a providing a tool for determining target occupancy of RAGE inhibitors. The findings outlined in this study and others[26] pave the way for the development of a second generation of RAGE PET radiopharmaceuticals with optimal lipophilicity profiles commensurate with improved *in vivo* imaging signal-to-noise ratios. Longitudinal studies determining the *in vivo* brain uptake in AD animal models using both RAGE and ß-amyloid PET radiotracers would enable the evaluation of RAGE as and early AD biomarker. assisting the discovery of new therapies. In the longer term, RAGE PET radiotracers may allow the development and evaluation of new disease-modifying treatments as well as an early diagnostic tool for AD.

SUMMARY POINTS

- The Receptor for Advanced Glycated Endproducts (RAGE) is involved in the neuroinflammatory pathway in Alzheimer's Disease (AD) and found to be overexpressed in early pre-AD pathology.
- FPS-ZM1, reported by Deane *at al.,* is a RAGE inhibitor which is able to restore cognitive function in AD mouse models (Tg2576). The radiolabelling of FPS-ZM1 would allow the imaging of *in vivo* RAGE expression and its early involvement with disease progression.
- [^{11}C]CO chemistry allows rapid radiolabelling of the amide moiety of FPS-ZM1. A novel [^{11}C]CO_2-to-[^{11}C]CO conversion *via* ^{11}C-silanecarboxylate derivatives was optimized and then applied to the radiolabeling of [^{11}C]FPS-ZM1.

- *In vitro* autoradiography studies with [^{11}C]FPS-ZM1 showed a non-statistically significant difference in specific binding in AD-mouse model (Tg2576) brains compared to wild-type mouse brains. A high non-displaceable binding was observed, probably due to the high lipophilicity of [^{11}C]FPS-ZM1.
- Follow-up studies using more hydrophilic probes to lower the non-displaceable binding are needed to correlate RAGE expression and early AD stages *in vivo*.

ABBREVIATIONS USED

[^{11}C] – carbon-11-labelled radiotracer; [^{11}C]CO – carbon-11 labelled carbon monoxide; [^{11}C]CO_2 – carbon-11 labelled carbon dioxide; [^{18}F] – fluorine-18-labelled radiotracer; Aβ – beta amyloid; AD – Alzheimer's disease; AGEs – advanced glycation endproducts; BACE1 - β-secretase enzyme 1; BBB – blood brain barrier; ^{11}C – carbon-11; EOB – end of bombardment; EOD – end of [^{11}C]CO_2 delivery; ^{18}F – fluorine-18; NDB – non-displaceable binding; NFT – neurofibrillary tangle; PET – positron emission tomography; RAGE – receptor for advanced glycation endproducts; RCP – radiochemical purity; RCY – radiochemical yield; ROI – region of interest; SB – specific binding; TB – total binding; TBAF – tetrabutyl ammonium fluoride; TG – transgenic; WT – wild-type;

CONFLICT OF INTEREST DISCLOSURE

The authors declare no competing financial interest.

ACKNOWLEDGMENTS

This work was supported by Medical Research Council [MRC, MR/K022733/1], European Commission, FP7-PEOPLE-2012-ITN [316882, RADIOMI] and the Wellcome/EPSRC Centre for Medical Engineering [WT 203148/Z/16/Z]. The research was supported by the

National Institute for Health Research (NIHR) Biomedical Research Centre based at Guy's and St Thomas' NHS Foundation Trust and King's College London. The views expressed are those of the authors and not necessarily those of the NHS, the NIHR or the Department of Health. The authors also acknowledge Dr. Richard Killick for providing the Tg2576 mouse brains.

REFERENCES

1. Beach TG, Phillips LE, Monsell SE, Kukull W. Accuracy of the Clinical Diagnosis of Alzheimer Disease at National Institute on Aging Alzheimer Disease Centers, 2005–2010. *J Neuropathol Exp Neurol.* 71(4), 266-273 (2012).
2. Shaik SS, Varma AR. Differentiating the dementias: a neurological approach. *Prog. Neurol. Psychiatry* 16(1), 11-18 (2012).
3. Ziegler SI. Positron Emission Tomography: Principles, Technology, and Recent Developments. *Nuclear Physics A* 752 679-687 (2005).
4. Nordberg A, Rinne JO, Kadir A, Långström B. The use of PET in Alzheimer disease. *Nat. Rev. Neurol.* 6 78 (2010).
5. Bateman RJ, Xiong C, Benzinger TL *et al*. Clinical and biomarker changes in dominantly inherited Alzheimer's disease. *N Engl J Med* 367(9), 795-804 (2012).
6. Vandenberghe R, Van Laere K, Ivanoiu A *et al*. 18F-flutemetamol amyloid imaging in Alzheimer disease and mild cognitive impairment: a phase 2 trial. *Ann Neurol* 68(3), 319-329 (2010).
7. Manook A, Yousefi BH, Willuweit A *et al*. Small-animal PET imaging of amyloid-beta plaques with [11C]PiB and its multi-modal validation in an APP/PS1 mouse model of Alzheimer's disease. *PLoS One* 7(3), e31310 (2012).
8. Rowe CC, Ellis KA, Rimajova M *et al*. Amyloid imaging results from the Australian Imaging, Biomarkers and Lifestyle (AIBL) study of aging. *Neurobiol Aging* 31(8), 1275-1283 (2010).
9. Annus T, Wilson LR, Hong YT *et al*. The pattern of amyloid accumulation in the brains of adults with Down syndrome. *Alzheimers Dement* 12(5), 538-545 (2016).
10. Morris E, Chalkidou A, Hammers A, Peacock J, Summers J, Keevil S. Diagnostic accuracy of (18)F amyloid PET tracers for the diagnosis of Alzheimer's disease: a systematic review and meta-analysis. *Eur J Nucl Med Mol Imaging* 43(2), 374-385 (2016).
11. Cohen JP, Dong J, Lu CY, Chakravarthy R. Restricting access to florbetapir: Medicare coverage criteria for diagnostics and drugs are inconsistent. *BMJ* 351 h3333 (2015).
12. James OG, Doraiswamy PM, Borges-Neto S. PET Imaging of Tau Pathology in Alzheimer's Disease and Tauopathies. *Front Neurol* 6 38 (2015).
13. Chien DT, Szardenings AK, Bahri S *et al*. Early clinical PET imaging results with the novel PHF-tau radioligand [F18]-T808. *J Alzheimers Dis* 38(1), 171-184 (2014).
14. Heutink P. Untangling tau-related dementia. *Hum Mol Genet* 9(6), 979-986 (2000).
15. Schwarz AJ, Yu P, Miller BB *et al*. Regional profiles of the candidate tau PET ligand 18F-AV-1451 recapitulate key features of Braak histopathological stages. *Brain* 139(Pt 5), 1539-1550 (2016).

16. **Bongarzone S, Savickas V, Luzi F, Gee AD. Targeting the Receptor for Advanced Glycation Endproducts (RAGE): A Medicinal Chemistry Perspective. *J Med Chem* 60(17), 7213-7232 (2017).**

**** A review describing the main biological and pharmacological aspects of RAGE.**

17. Sasaki N, Toki S, Chowei H *et al*. Immunohistochemical distribution of the receptor for advanced glycation end products in neurons and astrocytes in Alzheimer's disease. *Brain Res* 888(2), 256-262 (2001).
18. Deane R, Du Yan S, Submamaryan RK *et al*. RAGE mediates amyloid-beta peptide transport across the blood-brain barrier and accumulation in brain. *Nat Med* 9(7), 907-913 (2003).
19. Yan SD, Chen X, Fu J *et al*. RAGE and amyloid-beta peptide neurotoxicity in Alzheimer's disease. *Nature* 382(6593), 685-691 (1996).
20. Guglielmotto M, Aragno M, Tamagno E *et al*. AGEs/RAGE complex upregulates BACE1 via NF-κB pathway activation. *Neurobiol Aging* 33(1), 196.e113-196.e127 (2012).
21. **Deane R, Singh I, Sagare AP *et al*. A multimodal RAGE-specific inhibitor reduces amyloid beta-mediated brain disorder in a mouse model of Alzheimer disease. *J Clin Invest* 122(4), 1377-1392 (2012).**

**** *In vitro* and *in vivo* study of FPS-ZM1 pharmacological activity.**

22. Li XH, Lv BL, Xie JZ, Liu J, Zhou XW, Wang JZ. AGEs induce Alzheimer-like tau pathology and memory deficit via RAGE-mediated GSK-3 activation. *Neurobiol Aging* 33(7), 1400-1410 (2012).
23. Miller MC, Tavares R, Johanson CE *et al*. Hippocampal RAGE immunoreactivity in early and advanced Alzheimer's disease. *Brain Res* 1230 273-280 (2008).
24. Cui S, Xiong F, Hong Y *et al*. APPswe/Abeta regulation of osteoclast activation and RAGE expression in an age-dependent manner. *J. Bone Miner. Re.s* 26(5), 1084-1098 (2011).
25. Hsiao K, Chapman P, Nilsen S *et al*. Correlative memory deficits, Abeta elevation, and amyloid plaques in transgenic mice. *Science* 274(5284), 99-102 (1996).
26. **Cary BP, Brooks AF, Fawaz MV *et al*. Synthesis and Evaluation of [(18)F]RAGER: A First Generation Small-Molecule PET Radioligand Targeting the Receptor for Advanced Glycation Endproducts. *ACS Chem. Neurosci.* 7(3), 391-398 (2016).**

**** Development and *in vivo* testing of a fluorine-18, RAGE-targeting radiopharmaceutical.**

27. Kealey S, Gee A, Miller PW. Transition metal mediated [(11) C]carbonylation reactions: recent advances and applications. *J. Labelled Comp. Radiopharm.* 57(4), 195-201 (2014).
28. Rahman O. [^{11}C]Carbon monoxide in labeling chemistry and positron emission tomography tracer development: scope and limitations. *J. Labelled Comp. Radiopharm.* 58(3), 86-98 (2015).
29. Långström B, Itsenko O, Rahman O. [^{11}C]Carbon monoxide, a versatile and useful precursor in labelling chemistry for PET-ligand development. *J. Labelled Comp. Radiopharm.* 50(9-10), 794-810 (2007).
30. Zeisler SK, Nader M, Theobald A, Oberdorfer F. Conversion of No-carrier-added [^{11}C]carbon dioxide to [^{11}C]carbon monoxide on molybdenum for the synthesis of ^{11}C-labelled aromatic ketones. *Appl. Radiat. Isot.* 48(8), 1091-1095 (1997).
31. Anders DA, Bongarzone S, Fortt R, Gee AD, Long NJ. Electrochemical [^{11}C]CO_2 to [^{11}C]CO conversion for PET imaging. *Chem. Commun.* 53(20), 2982-2985 (2017).

32. **Taddei C, Bongarzone S, Haji Dheere AK, Gee AD. [^{11}C]CO_2 to [^{11}C]CO conversion mediated by [^{11}C]silanes: a novel route for [^{11}C]carbonylation reactions*. Chem. Commun.* 51(59), 11795-11797 (2015).**

**** The method for [^{11}C]CO production which was optimized in this manuscript.**

33. Flecknell P. Replacement, reduction and refinement. *ALTEX* 19(2), 73-78 (2002).
34. Dahl K, Schou M, Amini N, Halldin C. Palladium-Mediated [^{11}C]Carbonylation at Atmospheric Pressure: A General Method Using Xantphos as Supporting Ligand. *European Journal of Organic Chemistry* 2013(7), 1228-1231 (2013).
35. Laruelle M, Slifstein M, Huang Y. Relationships between radiotracer properties and image quality in molecular imaging of the brain with positron emission tomography. *Mol. Imaging Biol.* 5(6), 363-375 (2003).
36. Gee AD, Bongarzone S, Wilson AA. Small Molecules as Radiopharmaceutical Vectors. In: *Radiopharmaceutical Chemistry*, Lewis JS, Windhorst AD, Zeglis BM (Ed.^(Eds). Springer International Publishing Cham 119-136 (2019).
37. *Calculator Plugins were used for structure property prediction and calculation, Marvin Sketch 18.10, 2018, ChemAxon (http://www.chemaxon.com)*
38. Pike VW. PET radiotracers: crossing the blood-brain barrier and surviving metabolism. *Trends Pharmacol Sci* 30(8), 431-440 (2009).